SUPPLEMENTARY INFORMATION
Cellulose crystals plastify by localized shear

Gergely Molnár, David Rodney, Florian Martoïa, Pierre J. J. Dumont, Yoshiharu Nishiyama, Karim Mazeau, Laurent Orgéas

S1. Structure of I_β cellulose

Cellulose is made of D-glucose units shown in Fig. S1. The elementary structure contains 6 carbon, 5 oxygen and 12 hydrogen atoms. Carbon and oxygen atoms are indexed in Fig. S1 (O1 is the periodic image of O4). The dihedral angle describing the orientation of the exocyclic hydroxymethyl group, discussed in the main text, is defined by the sequence of atoms O5-C5-C6-O6.
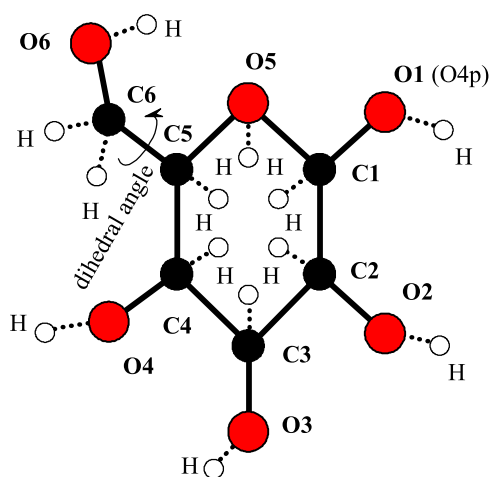

Fig. S1. D-glucose unit

I_β cellulose is the dominant crystalline structure present in wood and plant-based materials (1, 2). The individual glucose units form cellulose chains connected by $\beta(1 \rightarrow 4)$ glycosidic bonds. The chains are then layered in a staggered manner to form the structure shown in Fig. S2. One unit cell of I_β cellulose contains two chains referred to as center and corner chains after their respective positions. In a unit cell, each chain is made of 2 glucose units. More information about the structure can be seen in Ref. (1). The tilt angle in the xy plane was determined by the inclination of the unit vector respect to the y axis between the two following O2 atoms in the same chain segment in the crystalline unit.

We fitted the cellulose chains geometrically using an undulated ribbon-like volume shown in Fig. S3. The dimensions of the ribbons were taken according to the crystalline lattice constants in each direction and the amplitude of the sinusoidal undulations in the xz and yz planes are determined from the maximum separation between chains during shear deformation.

S2. Choice of the interatomic force field

Density Functional Theory (DFT) calculations are currently the most accurate method to model atomic interactions. However, such calculations are very computationally expensive and are limited to cells too small (a few tens to a hundred atoms (3)) to simulate localized shear deformations as studied in the main text. For this reason, we used a force field.

Dri et al. (4) have compared three different reactive force fields (ReaxFF) with two commonly-used non-reactive force fields (COMPASS™and GLYCAM) in terms of their ability to predict lattice parameters, elastic constants, coefficients of thermal expansion and anisotropy of cellulose I_β. None of the potentials was found able to predict accurately these properties. By way of contrast, the present force field, GROMOS 56A$_{carbo}$, is an open source potential specifically calibrated to reproduce most accurately both the structure and the stiffness of crystalline cellulose (4, 5).

With GROMOS, at 300 K and ambient pressure (1 atm), the unit vectors are $a = 0.7831$ nm, $b = 0.8074$ nm and $c = 1.0346$ nm, while experimentally Nishiyama et al. (1) obtained $a = 0.7784$ nm, $b = 0.8021$ nm and $c = 1.0380$ nm. The largest difference is thus 0.6 %. Also the thermal response of I_β crystals was studied recently with GROMOS, and good correlations were found with experiments (6). During yz shear, the conformation of the O5-C5-C6-O6 dihedral angle has a critical effect. Therefore, it is paramount that the potential describes the correct energy barriers between equilibrium states. GROMOS is the only potential where the torsional entropy was studied as a function of temperature (7) and where

Fig. S2. Interactive figure of monoclinic crystalline cellulose I$_\beta$.

excellent correlations were found with X-ray diffraction measurements. Additionally, both longitudinal ($E_L = 91.6$ GPa) and transversal ($E_T = 14.8$ GPa) elastic stiffnesses lie within the range of the experimental measurements: $E_L = 90 - 200$ GPa, $E_T = 15$ GPa (8).

S3. Local strain

The local strain tensor was calculated on a grid based on the displacements of the discrete atoms. First, in order to obtain a continuous displacement field, a 3D Gaussian coarse-graining function was used:

$$\phi\left(r\right) = \frac{1}{\pi^{3/2}w^3}e^{-(r/w)^2},$$ [1]

where w is the coarse-graining scale, which determines the width of the averaging. In the present case; we chose $w = 0.3$ nm. Then the continuous coarse-grained displacement field was calculated as:

$$\mathbf{u}\left(\mathbf{r}\right) = \frac{\sum\limits_{i=1}^{N}\mathbf{u}_i\phi\left(\|\mathbf{r} - \mathbf{r}_i\|\right)m_i}{\sum\limits_{i=1}^{N}\phi\left(\|\mathbf{r} - \mathbf{r}_i\|\right)m_i},$$ [2]

The summation is performed for every atom (N) within a cutoff ($r_{cut} = 3w$) range. $\mathbf{u}_i$, $\mathbf{r}_i$ and m_i are the atomic displacements, coordinates and masses respectively, while $\|\mathbf{r} - \mathbf{r}_i\|$ donates the distance between $\mathbf{r}_i$ and $\mathbf{r}$.

Finally to obtain the strains, the derivatives of the displacements were taken respect to the orthogonal directions:

$$\varepsilon_{\alpha\beta}\left(\mathbf{r}\right) = \frac{1}{2}\left(\frac{\partial u_\alpha\left(\mathbf{r}\right)}{\partial\beta} + \frac{\partial u_\beta\left(\mathbf{r}\right)}{\partial\alpha}\right),$$ [3]

Fig. S3. Geometrical fit of the corrugated ribbon on the cellulose chain.

where $(\alpha, \beta) = (x, y \text{ or } z)$. This representation is only meant to highlight localized shear zones, therefore a small strain assumption was considered sufficient.

Figs. S4 to S6 show local coarse-grained shear strain fields at different deformation stages along with the corresponding stress/strain curves. Before the first major plastic event, the deformation is homogeneous with shuffles inside the crystalline unit cells. However, after a stress drop, the shear deformation localizes between chains.
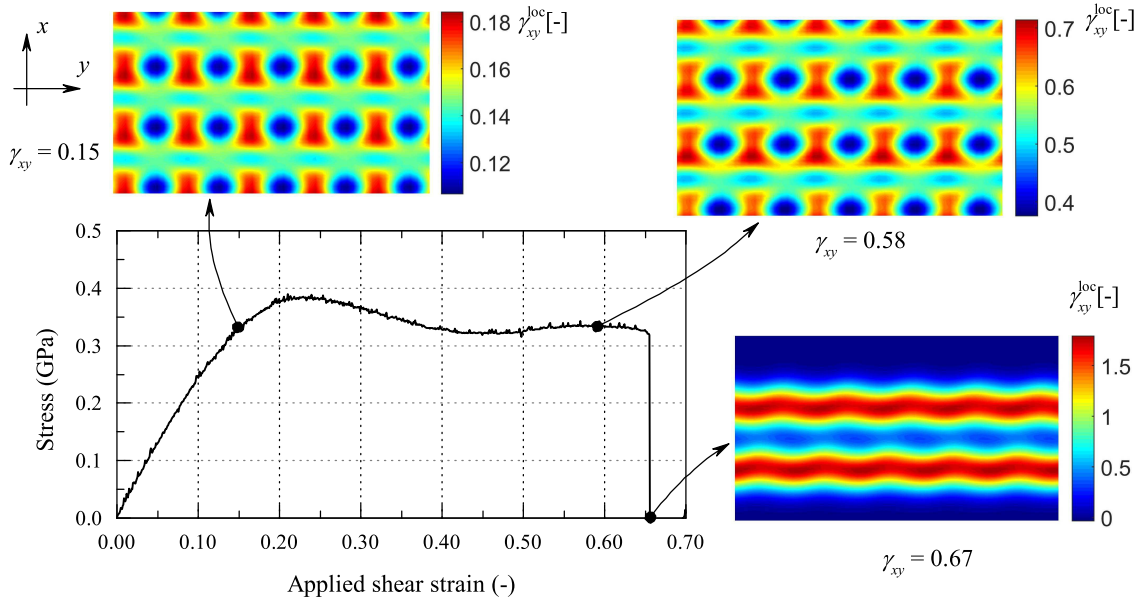

Fig. S4. Coarse-grained xy shear strain for xy shear deformation.

The coarse-graining technique was used only to visualize the local strain upon shear deformation. Naturally, the absolute value of the strain field depends on the chosen coarse-graining width (w in eq. 1) for a discrete system. Fig. S7 shows the local shear strain as a function of the coarse-graining width. It can be seen that the positions of the local maxima are unchanged. All shear bands appear in-between chains. We found no evidence of deformation of the cellulose chains themselves except the change of dihedral angle in the yz case. None of the C-O and C-C bonds exceeded by more than 0.08 % the equilibrium bond length (0.144 nm and 0.153 nm respectively). Moreover, none of the bond angles involving carbon and oxygen atoms deviated by more than $\pm 3°$ from the standard value (109.5°).

In Fig. S8, the coarse-grained local shear strain field is shown for the sample containing two dislocations. Initially, the deformation is homogeneous as in previous cases, however after reaching the elastic limit, the dislocations start to glide and localized shear bands appear between the dislocated planes.
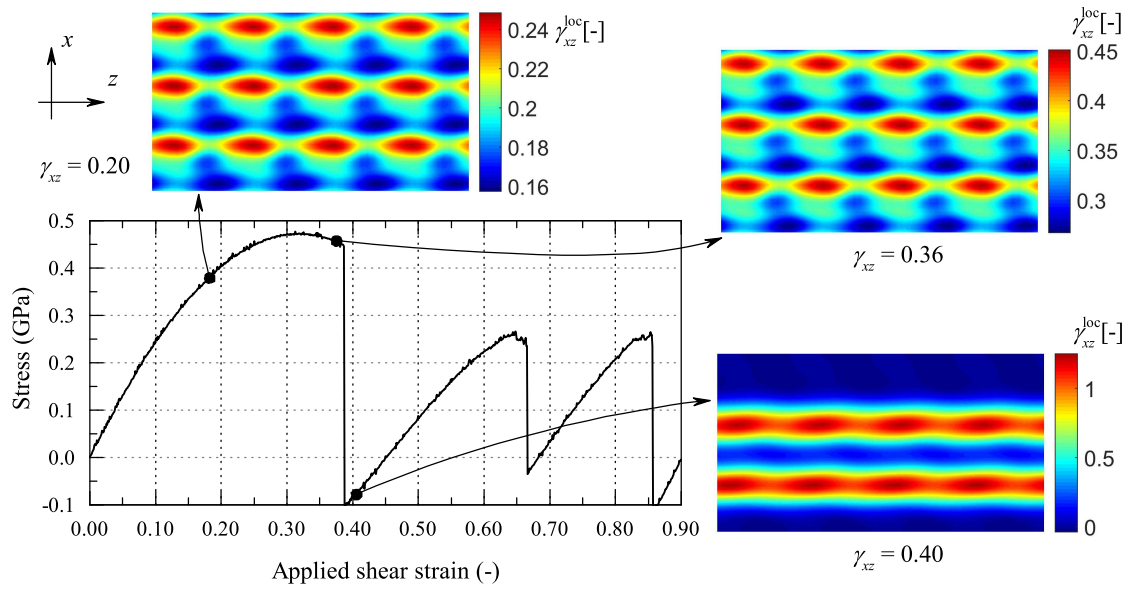
Fig. S5. Coarse-grained xz shear strain for xz shear deformation.
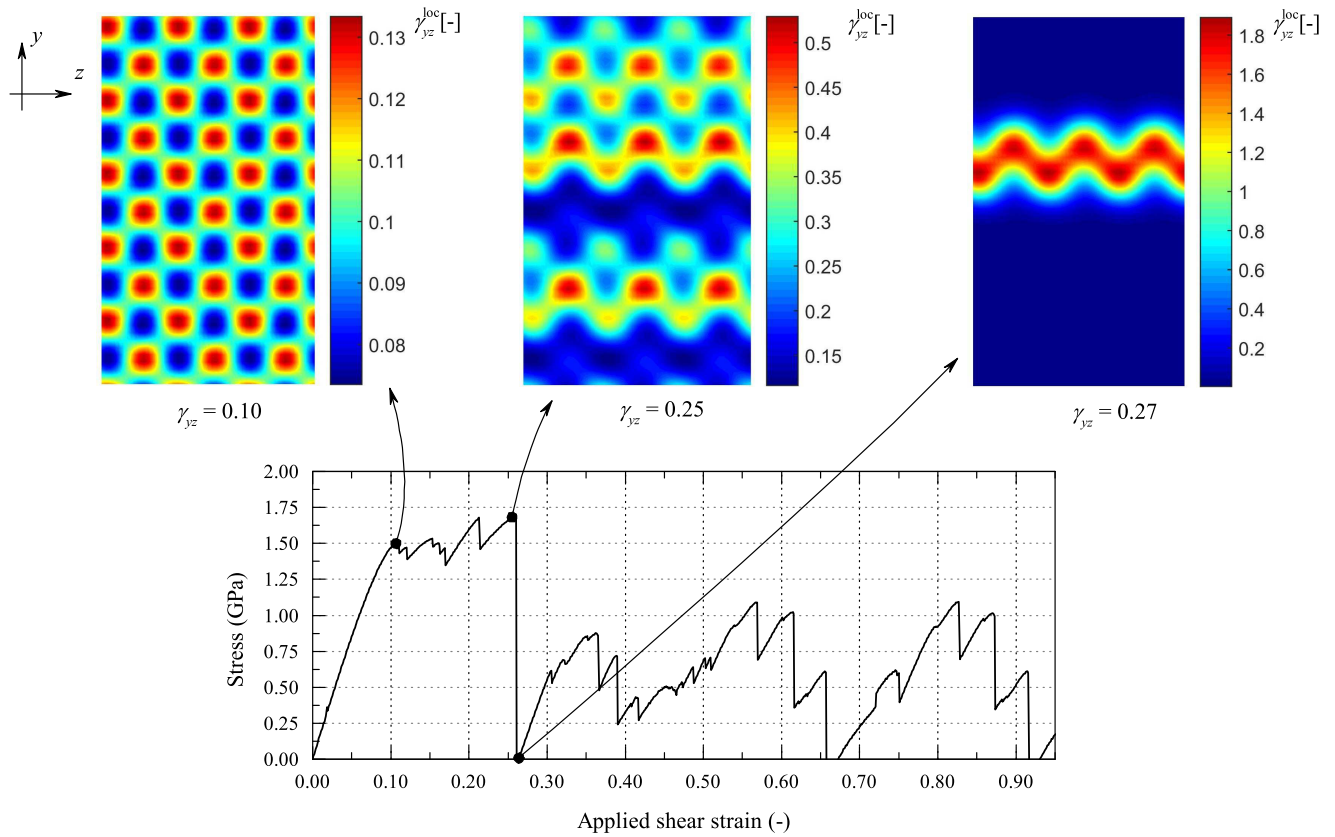

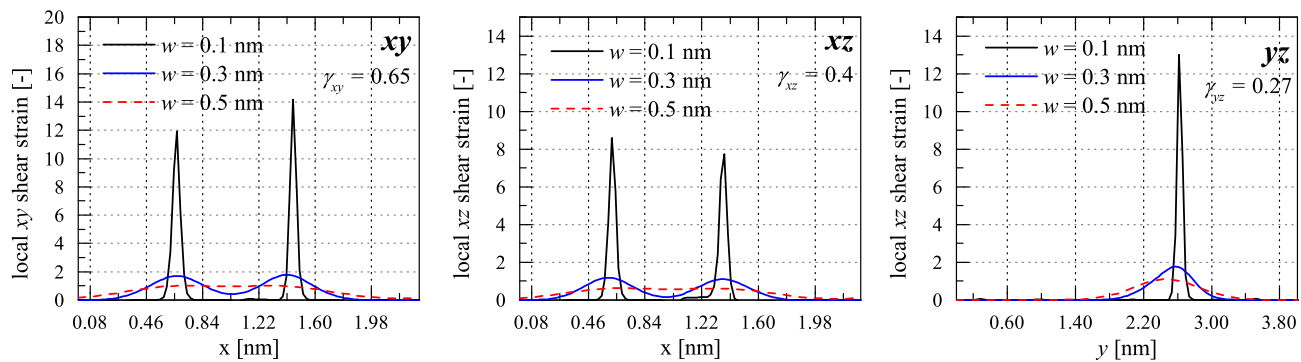**Fig. S6.** Coarse-grained yz shear strain for yz shear deformation.

Fig. S7. Local shear strain field along the height of the sample. Each curve was taken after a stress drop. The applied strain is indicated in the right corner. Dotted guidelines show the position of the centerline of each cellulose chain.
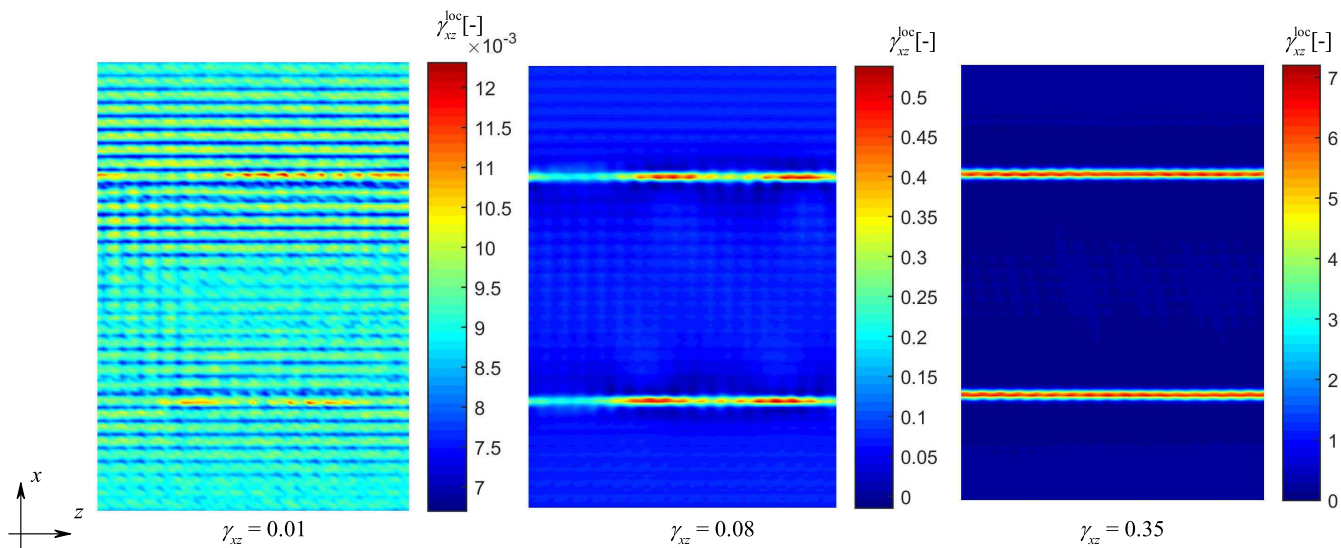

Fig. S8. Coarse-grained xz shear strain in the sample containing dislocations.

S4. Size effect

The effect of sample size was tested by increasing the in-plane size of the simulation box. For example to test the shear response in the xy plane, two larger systems were considered with $8a{\times}10b{\times}4c$ and $13a{\times}15b{\times}4c$ repetitions of the unit cell. Similarly, in the xz and the yz plane we used $8a{\times}5b{\times}9c$, $13a{\times}5b{\times}14c$ and $3a{\times}10b{\times}9c$, $3a{\times}15b{\times}14c$ respectively.
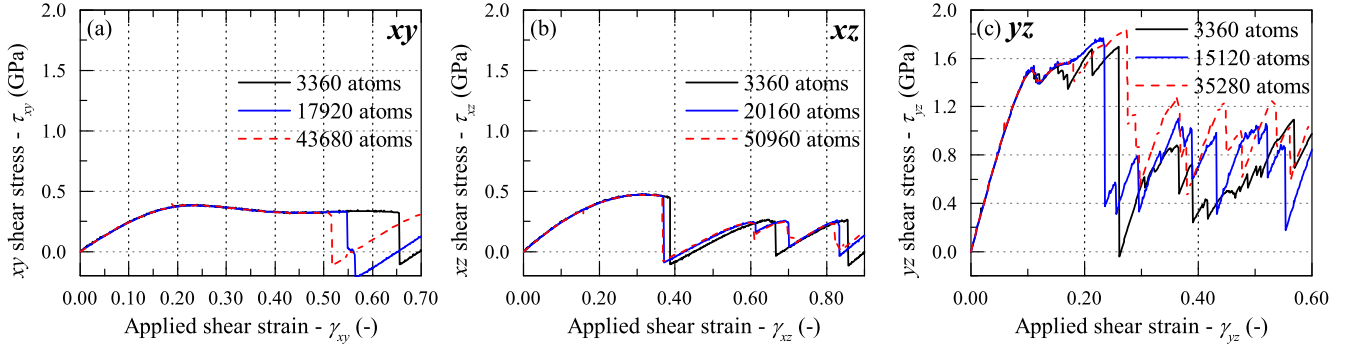

Fig. S9. Shear stress in different planes as a function of simulation box size.

First, changes to the cell dimensions does not change the atomic processes of deformation described in the main text. Also, it is shown in Fig. S9 that the strength (maximum shear stress) of the samples and the corresponding strain are independent of the box size. The stress drops corresponds to localized shear bands. The strain and therefore the stress drop per band is inversely proportional to the cell height, as discussed in the main text. Therefore, the stress drop per band decreases in larger simulation cells. However, the number of shear bands tends to increase, such that, the major stress drops are hardly affected by a change of simulation cell size, as seen in Fig. S9.

S5. Deformation localization

To intentionally initiate a shear band between two given planes, additional shear strain was applied inhomogeneously. As shown in Fig. S10, we defined three regions, two outer regions of height h_1 and h_3 and a central region (h_2) where we applied an extra strain increment $\delta\gamma^\ell$ while maintaining the global strain increment ($\delta\gamma = 10^{-3}$). To do so, we applied different strain increments in the three regions ($\delta\gamma_1^\ell$, $\delta\gamma_2^\ell$, $\delta\gamma_3^\ell$) expressed as:

$$\delta\gamma_1^\ell = \delta\gamma - \delta\gamma^\ell \frac{h_2}{h_1 + h_3}, \tag{4}$$

$$\delta\gamma_2^\ell = \delta\gamma + \delta\gamma^\ell, \tag{5}$$

$$\delta\gamma_3^\ell = \delta\gamma_1^\ell. \tag{6}$$

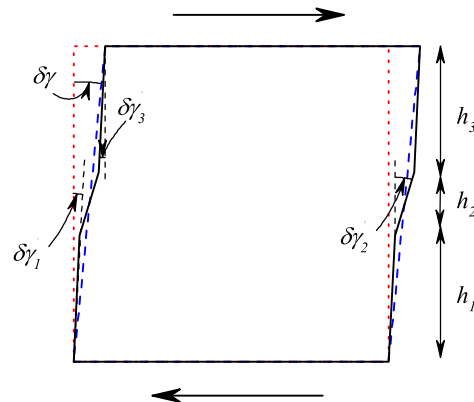In practice, we used $\delta\gamma^\ell = 10^{-3}$.

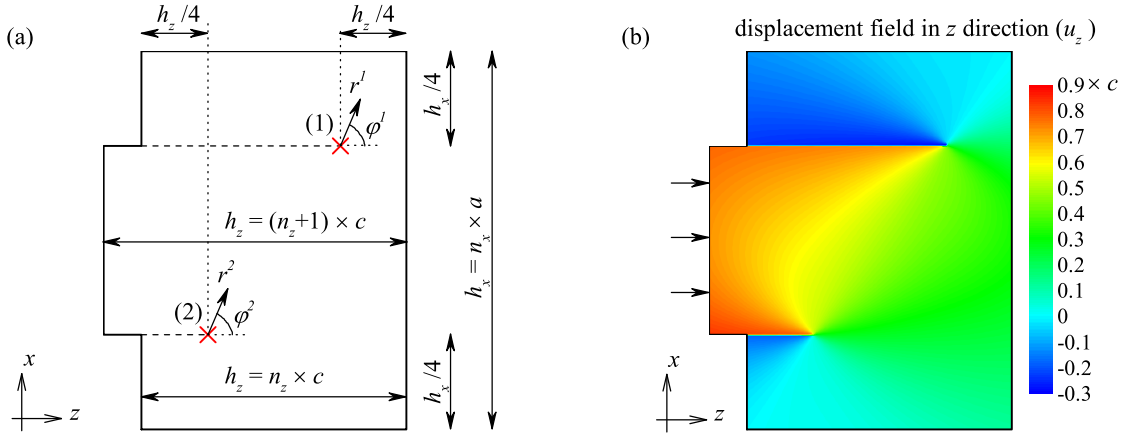**Fig. S10.** Inhomogeneously applied deformation to localize shear bands.

Fig. S11. (a) Schematic illustration of the position of the dislocations and the polar coordinate systems. (b) Applied displacement field in the z direction.

S6. Dislocation generation

To study the effect of structural defects in cellulose crystals, dislocations forming a dipole were generated at two positions between crystalline planes. To create these defects in a periodic system, an additional unit cell was added in the z direction to half of the sample to prepare for the extra half-plane inside the dislocation dipole. To regain periodicity, two displacement fields were applied on the whole sample from the positions of the dislocations cores based on elasticity theory (9)

Fig. S11(a) shows the initial configuration with the two dislocation cores highlighted by red crosses. The applied displacement fields in both z and x directions are expressed as:

$$u_z^i(r^i, \varphi^i) = \frac{b^i}{2\pi} \left(\varphi^i + \frac{\sin\left(2\varphi^i\right)}{4\left(1-\nu\right)} \right),$$ [7]

$$u_x^i(r^i, \varphi^i) = \frac{b^i}{2\pi} \left(\nu \log\left(r^i\right) + \frac{\cos\left(2\varphi^i\right)}{4\left(1-\nu\right)} \right),$$ [8]

where u_z^i and u_x^i are the displacement fields in directions z and x respectively. ν is Poisson's ratio, which was approximated to 0.33. However, this numerical value has no effect since the sample is equilibrated after introduction of the dislocations.

The position of each atom in the sample can be written in polar coordinates, where the pole for each coordinate system is the position of the dislocation cores and the angle φ^i is measured from the z axis. The distance between core i and an arbitrary atom is denoted r^i. Finally, b^i is the Burger's vector of dislocation i with values $-c$ and c (the crystalline lattice vector in the z direction). The two displacement fields are added:

$$u_x = \sum_{i=1}^{2} u_x^i, u_z = \sum_{i=1}^{2} u_z^i,$$ [9]

to generate the overall applied displacement field shown in Fig. S11(b). We see that the middle section of the cell is compressed, while the outer sections are extended. As a result, the initial steps disappear and we recover a simulation cell without steps and a length along z close to $(n_z + 0.5) \times c$. The length increase of $0.5c$ is physically due to the introduction of the dipole extra half-plane.

This initial configuration was then equilibrated with a conjugated gradient algorithm, then the same heating/cooling procedure was carried out as applied to the perfect crystals and described in the main text.

S7. Supplementary Movies

Captions for the Supplementary Movies:

S1_ShearXY.wmv
SM1: Atomic structure during the shear deformation in the xy plane. Green spheres indicate the atoms which were aligned initially.

S2_ShearXZ.wmv
SM2: Atomic structure during the shear deformation in the xz plane. Green spheres indicate the atoms which were aligned

initially.

S3_ShearYZ.wmv

SM3: Atomic structure during the shear deformation in the yz plane. Green spheres indicate the atoms which were aligned initially.

S4_ElementaryXY.wmv

SM4: Rotation of the cellulose chains around its z axis upon shear deformation in the xy plane.

S5_ElementaryXZ.wmv

SM5: Position of the cellulose chains during the localized shear deformation in the xz plane fitted with the corrugated shapes.

S6_ElementaryYZ.wmv

SM6: Position of the cellulose chains in the shear band during the shear deformation in the yz plane fitted with the corrugated shapes.

References

1. Nishiyama Y, Langan P, Chanzy H (2002) Crystal structure and hydrogen-bonding system in cellulose Iβ from synchrotron X-ray and neutron fiber diffraction. J Am Chem Soc 124(31):9074–9082.
2. Zugenmaier P (2008) Crystalline Cellulose and Derivatives. (Springer-Verlag Berlin Heidelberg).
3. Bučko T, Tunega D, Ángyán JG, Hafner J (2011) Ab initio study of structure and interconversion of native cellulose phases. The Journal of Physical Chemistry A 115(35):10097–10105.
4. Dri FL, Wu X, Moon RJ, Martini A, Zavattieri PD (2015) Evaluation of reactive force fields for prediction of the thermo-mechanical properties of cellulose Iβ. Computational Materials Science 109:330 – 340.
5. Chen P, Nishiyama Y, Mazeau K (2014) Atomic partial charges and one Lennard-Jones parameter crucial to model cellulose allomorphs. Cellulose 21(4):2207–2217.
6. Bergenstråhle M, Berglund LA, Mazeau K (2007) Thermal response in crystalline Iβ cellulose: A molecular dynamics study. The Journal of Physical Chemistry B 111(30):9138–9145.
7. Chen P, Nishiyama Y, Mazeau K (2012) Torsional entropy at the origin of the reversible temperature-induced phase transition of cellulose. Macromolecules 45(1):362–368.
8. Diddens I, Murphy B, Krisch M, Müller M (2008) Anisotropic elastic properties of cellulose measured using inelastic X-ray scattering. Macromolecules 41(24):9755–9759.
9. Bulatov V, Cai W, eds. (2006) Computer simulations of dislocations. (Oxford University Press, Oxford, England).